Chinese Chemical Letters 35 (2024) 108753

Contents lists available at ScienceDirect

Chinese Chemical Letters

journal homepage: www.elsevier.com/locate/cclet

Coupling WO_{3-x} dots-encapsulated metal-organic frameworks and template-free branched polymerization for dual signal-amplified electrochemiluminescence biosensing

Fei Yin[a], Erli Yang[a], Xue Ge[a], Qian Sun[a], Fan Mo[a], Guoqiu Wu[b,c], Yanfei Shen[a,b,c,*]

[a] Medical School, Southeast University, Nanjing 210009, China
[b] Center of Clinical Laboratory Medicine, Zhongda Hospital, Southeast University, Nanjing 210009, China
[c] Jiangsu Provincial Key Laboratory of Critical Care Medicine, Southeast University, Nanjing 210009, China

ARTICLE INFO

Article history:
Received 11 March 2023
Revised 8 June 2023
Accepted 28 June 2023
Available online 30 June 2023

Keywords:
Dual signal-amplified electrochemiluminescence
WO_{3-x} dots
MOFs
Template-free branched polymerization
DNA methyltransferase

ABSTRACT

Developing accurate and sensitive DNA methyltransferase (MTase) analysis methods is essential for early clinical diagnosis and development of antimicrobial drug targets. In this work, by coupling WO_{3-x} dots-encapsulated metal-organic frameworks (MOFs) as co-reactants and terminal deoxynucleotidyl transferase (TdT)-mediated template-free branched polymerization, a dual signal-amplified electrochemiluminescent (ECL) biosensor was constructed to detect DNA adenine methylation (Dam) MTase. The employment of WO_{3-x} dots-encapsulated MOFs (*i.e.*, NH_2-UIO66@WO_{3-x}) was not only beneficial for biomolecule conjugation because of the abundant amino groups but also led to a 7-fold enhanced ECL response due to the increased loading of WO_{3-x}. Moreover, TdT-mediated template-free branched polymerization promoted the capture of ECL emitters on the electrode surface, achieving 20-fold enhanced signal amplification. The presented ECL biosensor demonstrated a low detection limit of 2.4×10^{-4} U/mL, and displayed high reliability for the detection of Dam MTase in both spiked human serum and *E. coli* cell samples, and for the screening of potential inhibitors. This study opens a new avenue for designing a dual signal amplification-based ECL bioassay for Dam MTase and screening inhibitors in the fields of clinical diagnosis and drug development.

DNA methyltransferase (MTase) widely exists in biological organisms and can catalyze methylation reactions, which transfer cytosine or adenine bases in specific DNA with S-adenosyl-L-methionine (SAM) as a methyl donor [1,2]. From prokaryotes to eukaryotes, many major physiological processes are involved in the regulation of methyltransferases [3]. In humans, DNA MTase is a crucial component in gene expression, genome maintenance, and parental imprinting and its overexpression may be closely related to the occurrence and progression of various cancers [4–6]. In bacterial species, DNA MTase participates in the regulation of bacterial virulence and motility, and is a critical factor for bacterial colonization of hosts to cause disease [7–9]. Hence, DNA MTase may serve as a typical diagnostic biomarker as well as a target for antimicrobial drugs [10,11]. Recently, many methods have been available for determining DNA MTase activity, including colorimetry [12], fluorescence [13], electrochemistry [14] and photoelectrochemistry [15]. However, the quantitative determination of DNA MTase with high sensitivity remains challenging owing to the instability of detection probes and the complexity of detection procedures. Therefore, it is important to construct develop a highly accurate and sensitive and specific biosensor method for detecting the activity of DNA MTases and screening inhibitors.

Electrochemiluminescence (ECL) is a process that forms high-energy excited states from luminescent substances through electrochemical reactions on the electrode surface and then relaxes to the ground states, emitting light [16–19]. Because ECL fully integrates the merits of electrochemistry and chemiluminescence, it is a promising technology with high sensitivity, controllable luminescence, and easy miniaturization [20–22]. In particular, the co-reactant-type ECL is widely employed in biomedical analysis and clinical diagnosis, where co-reactants play an extremely significant role [17,23-25]. However, current commercial co-reactants such as tripropylamine (TPrA) possess gross dilemmas, such as high biotoxicity and strong background signals in the anodic ECL reaction [26,27]. As a result, it is highly desirable to explore alternative ECL co-reactants.

---

[*] Corresponding author.
E-mail address: Yanfei.Shen@seu.edu.cn (Y. Shen).

https://doi.org/10.1016/j.cclet.2023.108753
1001-8417/

Semiconductor quantum dots such as WO_{3-x} dots show great potential in the field of ECL because of their low cost, ease of preparation, stable performance, and tunable size [28]. However, the lack of active groups for linking biomolecules hinders their broad application in bioassays [28]. Recently, surface functionalization with polymers or inorganic materials has been regarded as an effective way to improve the ability to couple with biomolecules and accommodate guest-active nanomaterials [29–35]. Metal-organic frameworks (MOFs) are one of the most popular materials with large specific surface areas, high porosities, and tunable chemical properties [36–39], allowing them to encapsulate guest molecules effectively [40–42]. On the other hand, MOFs can be conveniently conjugated with biomolecules by selecting suitable organic ligands with reactive terminal groups [43,44]. Therefore, MOFs can be a desirable candidate to accommodate WO_{3-x} dots for the preparation of highly efficient co-reactants for ECL bioanalysis.

Herein, a dual signal-amplified ECL biosensor was constructed by coupling the co-reactants of WO_{3-x} dots-encapsulated MOFs (NH_2-UIO66@WO_{3-x}) with terminal deoxynucleotidyl transferase (TdT)-mediated template-free branched polymerization for quantitative determination of DNA adenine methylation (Dam) MTase, a type of DNA MTase. The employment of NH_2-UIO66@WO_{3-x} was not only beneficial for biomolecule conjugation because of the abundant amino groups, but also led to an elevated ECL response ascribed to the enhanced loading of WO_{3-x} by NH_2-UIO66. Moreover, the use of branched double-stranded DNA (dsDNA) instead of traditional linear dsDNA for TdT-mediated template-free branched polymerization promoted the capture of ECL emitters, resulting in enhanced signal amplification. The developed biosensor achieved a low detection limit of 2.4×10^{-4} U/mL, and was successfully applied for screening inhibitors and determining Dam MTase in spiked serum samples and *E. coli* cells with high reliability. This study offers a new strategy for designing a dual signal-amplified ECL biosensor for the sensitive determination of Dam MTase activity and screening inhibitors for clinical diagnosis and drug development.

The NH_2-UIO66@WO_{3-x} nanocomposites were synthesized *via* a facile two-step procedure (Fig. 1a). The transmission electron microscopy (TEM) image showed WO_{3-x} dots with excellent monodispersity in aqueous solution exhibited average size of 2.82±0.66 nm (Fig. 1b) and an interplanar *d* spacing of 0.37 nm. WO_{3-x} dots with hydroxyl groups were immobilized on protonated NH_2-UIO66 with a regular octahedral nanostructure (Fig. 1c) through electrostatic interactions. After complexation with WO_{3-x}, the resulting NH_2-UIO66@WO_{3-x} nanocomposites retained their original shape of NH_2-UIO66 with tiny amount of nanoparticles on the surface (Fig. 1d). The EDS mapping analysis showed that N, Zr, and W were uniformly distributed in the nanocomposites (Fig. S1 in Supporting information). Elemental line scanning analysis (Fig. 1e) demonstrated that W was found throughout the nanostructure, suggesting that WO_{3-x} dots were distributed mainly in the pores of NH_2-UIO66, and the small number of nanoparticles around the NH_2-UIO66 nanostructure were also WO_{3-x} dots.

The X-ray photoelectron spectroscopy (XPS) was applied for investigating the bonding information of NH_2-UIO66@WO_{3-x} nanocomposites. The typical peaks of O 1s, C 1s, N 1s, Zr 3d and W 4f were observed for NH_2-UIO66@WO_{3-x} as illustrated in Fig. 2a. The fitting curve of W 4f spectrum showed two spin-orbit doublets correlating to W^{6+} and W^{5+} (Fig. 2b), which was consistent with those of individual WO_{3-x} dots (Fig. S2 in Supporting information), indicating the presence of WO_{3-x} dots in the nanocomposites [45,46]. Moreover, the deconvoluted Zr 3d spectrum of the NH_2-UIO66@WO_{3-x} nanocomposites showed two strong peaks at 182.9 and 185.3 eV (Fig. 2c), which were attributed to Zr $3d_{5/2}$ and Zr $3d_{3/2}$, respectively (Fig. S3 in Supporting information) [47–49],

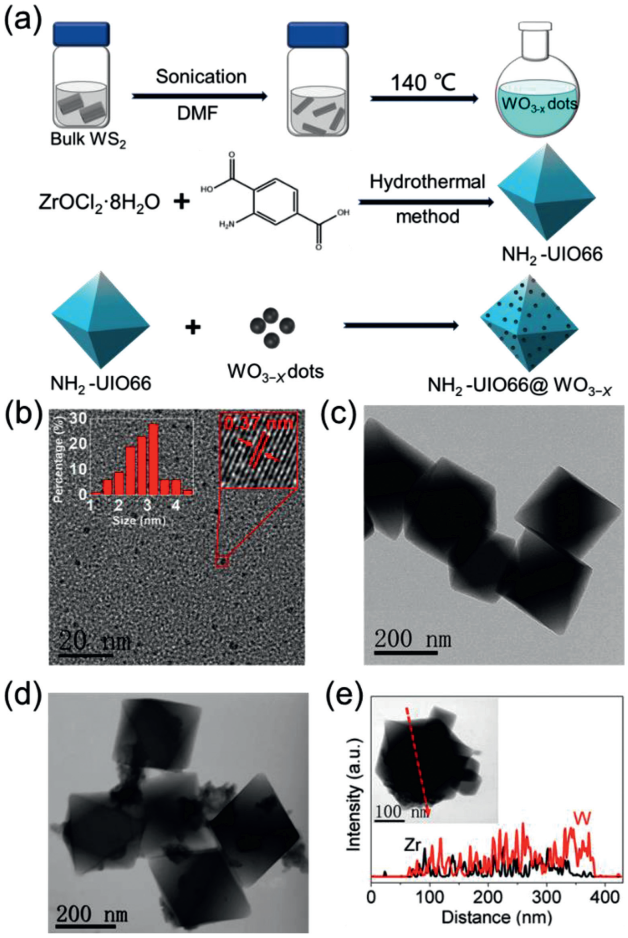

Fig. 1. (a) Scheme for the preparation of NH_2-UIO66@WO_{3-x}. TEM images of (b) WO_{3-x} dots, (c) NH_2-UIO66 and (d) NH_2-UIO66@WO_{3-x}. (e) Elemental line scan of a single NH_2-UIO66@WO_{3-x} particle indicated by the dashed line in the inset. Inset in (b): Size distribution of the WO_{3-x} dots.

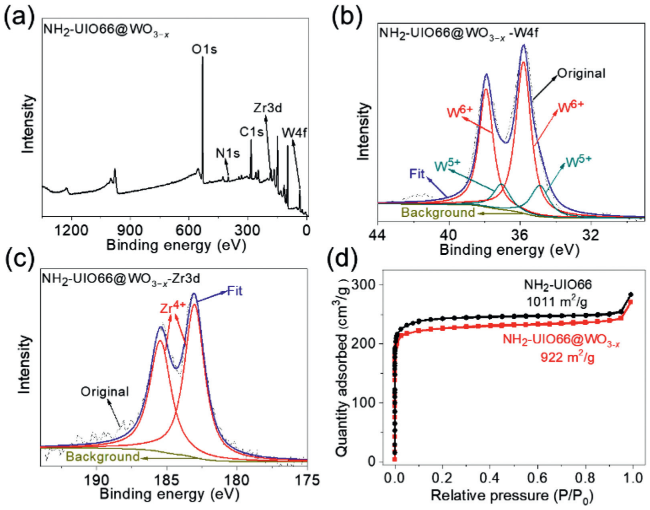

Fig. 2. (a) XPS survey spectrum of NH_2-UIO66@WO_{3-x}. Narrow XPS scan spectra of (b) W 4f and (c) Zr 3d spectra of NH_2-UIO66@WO_{3-x}. (d) N_2 adsorption-desorption isotherms curves of NH_2-UIO66@WO_{3-x} and NH_2-UIO66.

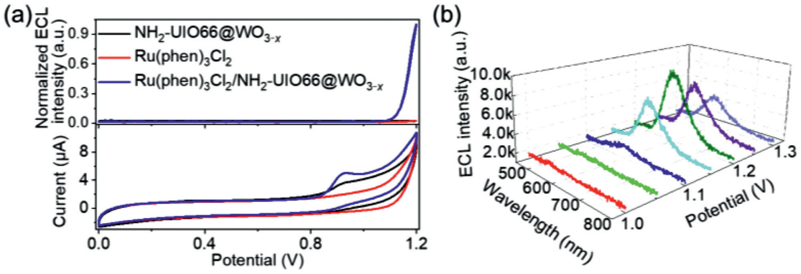

Fig. 3. (a) ECL-potential and CV curves of GCE in 0.1 mol/L PBS (pH 7.4) containing 0.5 mg/mL NH_2-UIO66@WO_{3-x}, 50 mmol/L $Ru(phen)_3Cl_2$, and the mixture of 50 mmol/L $Ru(phen)_3Cl_2$ and 0.5 mg/mL NH_2-UIO66@WO_{3-x}. (b) ECL spectra of $Ru(phen)_3Cl_2$/NH_2-UIO66@WO_{3-x} in 0.1 mol/L PBS (pH 7.4) collected at different potentials.

suggesting the presence of NH_2-UIO66 in the nanocomposites. Fourier Transform infrared spectroscopy (FTIR) results further verified the presence of both NH_2-UIO66 and WO_{3-x}. As shown in Fig. S4 (Supporting information), the FTIR spectrum of NH_2-UIO66@WO_{3-x} displayed a broad characteristic peak at 3475 cm^{-1}, assigned to N–H symmetric and asymmetric stretching vibrations, and two peaks at 1659 and 1569 cm^{-1}, assigned to the Zr^{4+}-coordinated COOH [50,51]. Moreover, the peak at 1252 cm^{-1} was related to the C–N stretching vibration of aromatic amines from NH_2-UIO66 [48,49,52]. Notably, the sharp absorption peaks at 806, 896, and 961 cm^{-1} were attributed to W-O bending and asymmetric and tensile vibrations of the WO_{3-x} dots, respectively [46]. Thermogravimetric analysis (TGA) demonstrated that the mass percentage of WO_{3-x} dots in NH_2-UIO66@WO_{3-x} was greater than 20% (Fig. S5 in Supporting information). Thus, these results demonstrated the successful synthesis of the NH_2-UIO66@WO_{3-x} nanocomposites.

To obtain more structural information on the NH_2-UIO66@WO_{3-x} nanocomposites, the surface areas of NH_2-UIO66@WO_{3-x} and NH_2-UIO66 were evaluated by N_2 adsorption-desorption isotherms (Fig. 2d). The surface areas of NH_2-UIO66@WO_{3-x} and NH_2-UIO66 were calculated as 922 m^2/g and 1011 m^2/g, respectively. The pore size distribution results (Fig. S6 in Supporting information) showed two kinds of pores in the range of 0.5–0.8 nm (tetrahedral microporous cages) and 1–1.5 nm (octahedral microporous cages) by density functional theory (DFT) [53,54]. After the complexation with WO_{3-x} dots, the pore volumes reduced slightly, which might be due to the fact the WO_{3-x} dots occupied or blocked the cavities of the NH_2-UIO66 [55].

$Ru(phen)_3Cl_2$, a typical ECL emitter, which can be embedded in the groove of dsDNA *via* electrostatic and covalent interactions [56,57], was selected for the biosensor fabrication. As shown in Fig. 3a, the anodic ECL signal of $Ru(phen)_3Cl_2$/NH_2-UIO66@WO_{3-x} was much higher than that of $Ru(phen)_3Cl_2$ alone, and NH_2-UIO66@WO_{3-x} alone did not exhibit an evident ECL signal, indicating the co-reactant effect of NH_2-UIO66@WO_{3-x} on the ECL of $Ru(phen)_3Cl_2$. The mass ratio of NH_2-UIO66: WO_{3-x} dots was further optimized at 1:1 for the preparation of the NH_2-UIO66@WO_{3-x} nanocomposites (Fig. S7 in Supporting information). It is noteworthy that the ECL signal of $Ru(phen)_3Cl_2$/NH_2-UIO66 was similar to that of $Ru(phen)_3Cl_2$ alone, and was negligible compared to $Ru(phen)_3Cl_2$/NH_2-UIO66@WO_{3-x} (Fig. S8 in Supporting information), suggesting a co-reactant effect of WO_{3-x} dots. To explore the mechanism of the $Ru(phen)_3Cl_2$/NH_2-UIO66@WO_{3-x} ECL system, the oxidation behavior of $Ru(phen)_3Cl_2$ and NH_2-UIO66@WO_{3-x} in PBS was investigated by cyclic voltammetry (CV), and the ECL-potential curves were recorded. As shown in Fig. 3a, the onset oxidation potentials of $Ru(phen)_3Cl_2$ and NH_2-UIO66@WO_{3-x} were at approximately 1.07 V and 0.77 V, respectively, indicating that NH_2-UIO66@WO_{3-x} was more easily oxidized than $Ru(phen)_3Cl_2$. Moreover, the ECL spectra of $Ru(phen)_3Cl_2$/NH_2-UIO66@WO_{3-x} collected at different potentials (Fig. 3b) suggested an onset potential at 1.1 V and a peak wavelength at approximately 600 nm, attributed to the emission of $Ru(phen)_3Cl_2$ (Fig. S9 in Supporting information), demonstrating that the generation of an ECL signal was after the time that both $Ru(phen)_3Cl_2$ and NH_2-UIO66@WO_{3-x} were oxidized. Along this line, it could be concluded that the ECL reaction of $Ru(phen)_3Cl_2$/NH_2-UIO66@WO_{3-x} was driven by an "oxidation–reduction" co-reaction route [58,59]. A linear relationship between the oxidation peak current and $\nu^{1/2}$ and the ECL peak intensity and $\nu^{1/2}$ was observed, respectively, indicating a typical diffusion-controlled process (Fig. S10 in Supporting information) [59]. Thus, it was preliminarily inferred that the ECL reaction mechanism of the $Ru(phen)_3Cl_2$/NH_2-UIO66@WO_{3-x} system was described in Scheme S1 (Supporting information).

Based on the excellent ECL-promoting performance of NH_2-UIO66@WO_{3-x} for the $Ru(phen)_3{}^{2+}$-ECL system, a signal-amplified ECL biosensor for Dam MTase was constructed using NH_2-UIO66@WO_{3-x} as a co-reactant. As shown in Fig. 4a, in the presence of Dam MTase, a palindromic probe was methylated at the adenine base and then specifically cleaved by the endonuclease DpnI, releasing DNA fragments with 3′-OH terminals. After the modification of NH_2-UIO66@WO_{3-x} nanocomposites onto GCE (NH_2-UIO66@WO_{3-x}/GCE), the released DNA fragments were covalently linked to NH_2-UIO66@WO_{3-x} on GCE *via* the -CO–NH- bond. The exposed 3′-OH terminals were then extended with dATP *via* TdT-mediated template-free polymerization to form poly-A chains [60], which subsequently hybridized with free poly-T fragments. Moreover, all the anchored poly-T fragments were continuously extended *via* TdT-mediated template-free polymerization to produce generous branched long poly-A chains, which were further hybridized with more free poly-T fragments. After multiple rounds of extension and assembly, a branched dsDNA nanostructure was formed on the NH_2-UIO66@WO_{3-x} modified GCE surface. It should be noted that with template-free branched polymerization, the branched dsDNA nanostructures can capture more ECL emitters of $Ru(phen)_3Cl_2$ onto the electrode surface to boost the ECL signal, and the ECL intensity of $Ru(phen)_3Cl_2$ can be correlated to the amount of Dam MTase in the biosensing system.

The feasibility of TdT-mediated branched template-free polymerization was verified using polyacrylamide gel electrophoresis (PAGE) in Fig. S11 (Supporting information). The eletrophoresis band was obtained for the renatured palindromic probe (Lane 2). In the presence of Dam MTase and SAM (Lane 3), the band of the palindromic probe disappeared, and a new band was observed, indicating that the methylated palindromic probe was digested and new DNA fragments were released. Upon the addition of TdT and dATP, a new band with a significantly enhanced molecular weight was obtained (Lane 1), which could be ascribed to TdT-mediated template-free polymerization and the formation of long linear dsDNA. It is worth noting that all the anchored poly-T fragments can be continuously extended by TdT-mediated template-free polymerization, generating generous branched long poly-A chains, which will hybridize with more free poly-T fragments to form branched

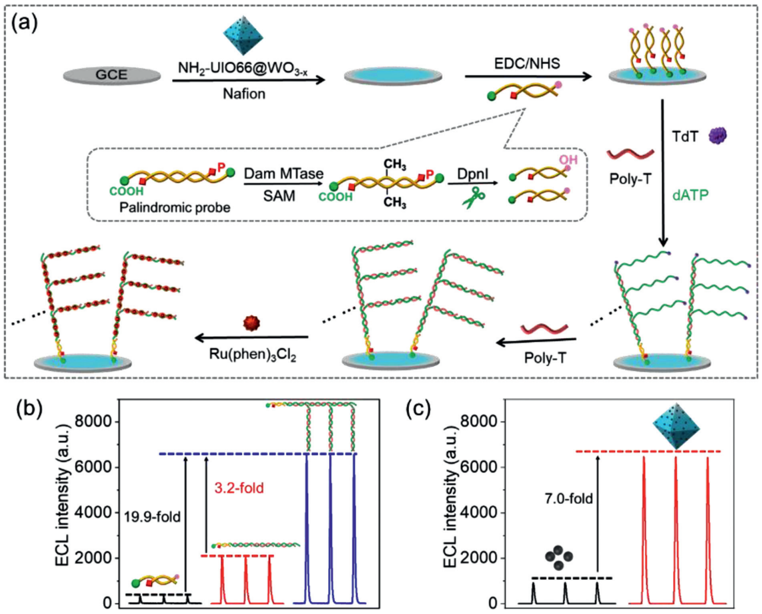

Fig. 4. (a) Scheme for the construction of the proposed ECL biosensor. (b) ECL response of the biosensor fabricated with different amplification reactions in 0.1 mol/L PBS (pH 7.4). Black line: without polymerization; red line: linear polymerization; blue line: branched polymerization. (c) ECL response of the sensing system using WO_{3-x} dots (black line) and NH_2-UIO66@WO_{3-x} (red line) as co-reactants in 0.1 mol/L PBS (pH 7.4). Potential scanning: 0 to 1.2 V, scan rate: 0.2 V/s, PMT: 800 V.

dsDNA. As a result, after multiple rounds of extension and assembly, as described above, a new band with a higher molecular weight appeared in the TdT-mediated branched polymerization (Lane 4). It should be noted that the TdT-mediated branched polymerization resulted in a 20-fold enhanced ECL response compared to that without polymerization and a 3.2-fold signal enhancement compared to that with linear polymerization (Fig. 4b). On the other hand, compared with individual WO_{3-x} dots, NH_2-UIO66@WO_{3-x} was not only beneficial for biomolecule conjugation because of the abundant amino groups on NH_2-UIO66, but also showed a 7-fold enhanced ECL response due to the increased loading of WO_{3-x} by NH_2-UIO66 (Fig. 4c). Thus, coupling TdT-mediated branched polymerization with NH_2-UIO66@WO_{3-x} would result in dual signal amplification for biosensing.

The assembly of the biosensor was confirmed by CV and electrochemical impedance spectroscopy (EIS). As shown in Fig. S12a (Supporting information), the CV of bare GCE in 0.1 mol/L PBS (pH 7.4) containing 2 mmol/L $[Fe(CN)_6]^{3-}$ displayed a pair of redox peaks with a peak potential difference of less than 85 mV, indicative of a reversible redox reaction. After NH_2-UIO66@WO_{3-x} was modified on the GCE, the peak current decreased obviously, ascribed to the poor electron conductivity of NH_2-UIO66@WO_{3-x}. After the covalent immobilization of DNA and the subsequent TdT-mediated branched polymerization reaction of DNA on the electrode, the peak current further decreased gradually because of the blocked electron transfer of $K_3Fe(CN)_6$ by DNA. After the intercalation of $Ru(phen)_3Cl_2$ into dsDNA, the peak current increased slightly, probably because of the mediating role of $Ru(phen)_3Cl_2$ on the electrode for electron transfer between the electrode and $K_3Fe(CN)_6$ in the solution. These results demonstrated the successful construction of the biosensor, which was consistent with the EIS results (Fig. S12b in Supporting information).

Under the optimized conditions (Fig. S13 in Supporting information), the ECL response of the dual signal-amplified biosensor for Dam MTase was recorded in the concentration from 1×10^{-3} U/mL to 100 U/mL (Fig. 5a). With increasing the Dam MTase concentration (Fig. 5b), a desirable linear relationship between the ECL signal (I) and the logarithm of Dam MTase concentration ($\lg C_{\text{Dam MTase}}$) was obtained as $I = 1119.7\ \lg C_{\text{Dam MTase}} + 4292.1$ ($R^2 = 0.991$), and the limit of detection (LOD) was calculated as 2.4×10^{-4} U/mL. The performance of the established biosensor was comparable to or superior to that of most of the previously reported detection methods (Table S1 in Supporting information).

The specificity of the constructed biosensing system was explored by using the M.SssI MTase as the interference protein and the single component of Dam MTase or DpnI as interference control. As shown in Fig. 5c, the ECL responses to Dam MTase, DpnI and M.SssI + DpnI were negligible compared to those of Dam MTase + DpnI, indicating that this biosensor is highly selective for Dam MTase analysis. Moreover, the ECL signal fluctuation of the proposed biosensor was negligible after 10 cycles of continuous scanning, with a relative standard deviation (RSD) of 0.62% (Fig. 5d). The stability was investigated by collecting the ECL signal of the constructed biosensor after a storage of 1, 3, 7, and 14 days at 4 °C, and 88.3% of the initial signal was observed after 14 days (Fig. S14 in Supporting information), thereby demonstrating the high stability of the biosensor.

The practical feasibility of the system was evaluated *via* recovery experiments by adding the Dam MTase standard into 10% diluted human serum samples, and the Dam MTase concentration was calculated using the standard curve shown in Fig. 5b. As shown in Table S2 (Supporting information), the recovery of Dam MTase was in the range of 96.45%–103.41%, with an RSD of less than 6.99%, indicating that the constructed biosensing system was applicable for complex biological samples. In addition, JM110 and DH5α *E. coli* cells were used as negative and positive samples to determine Dam MTase activity, respectively [61,62]. As shown in Fig. S15 (Supporting information), both the PBS and JM110 cell groups displayed negligible ECL signals, whereas the ECL signal of the DH5α cell group, which contained endogenous Dam MTase, was much higher, further verifying the practical feasibility of the as-constructed biosensing system.

Precise screening of targeted DNA MTase inhibitors opens up new channels for clinical treatment and drug development. The Dam MTase inhibition assay was performed using gentamicin, penicillin, and 5-fluorouracil as inhibitors [63–65]. The results showed that all three inhibitors could inhibit Dam MTase activity (Fig. 6a). It was found that 5-fluorouracil was more effective in in-

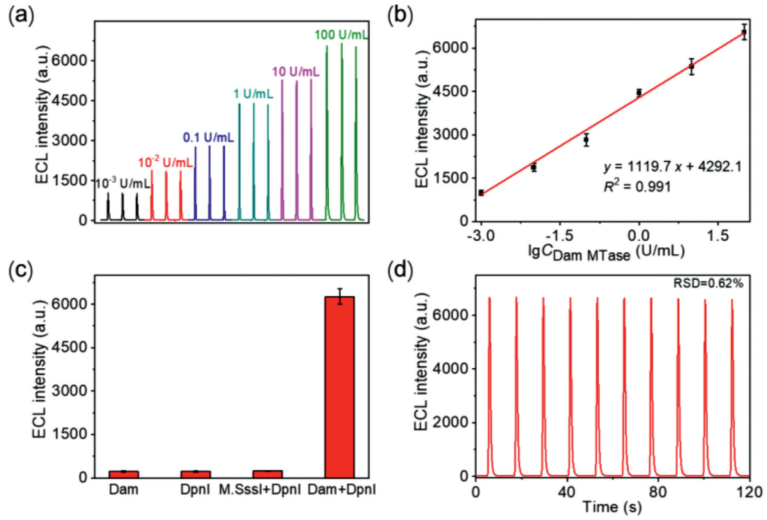

Fig. 5. (a) ECL response of the biosensor to different concentrations of Dam MTase in 0.1 mol/L PBS (pH 7.4) containing 80 U/mL DpnI. (b) Calibration curve of the ECL biosensor for Dam MTase. (c) ECL response of the proposed biosensor to Dam MTase, DpnI, M.SssI MTase + DpnI and Dam MTase + DpnI under the same experimental conditions. (d) Signal stability of the biosensor for 10 U/mL of Dam MTase under 10 continuous scanning cycles in 0.1 mol/L PBS (pH 7.4) containing 80 U/mL DpnI. Potential scanning: 0 to 1.2 V, scan rate: 0.2 V/s, PMT: 800 V.

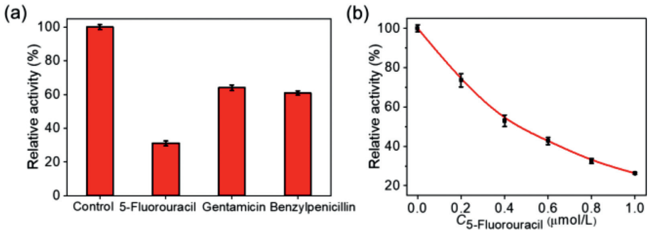

Fig. 6. (a) Inhibitory effect of 1 μmol/L of different inhibitors on Dam MTase activity (100 U/mL). (b) Inhibitory effect of different concentrations of 5-fluorouracil on Dam MTase activity (100 U/mL). Potential scanning: 0 to 1.2 V, scan rate: 0.2 V/s, PMT: 800 V.

hibiting the Dam MTase activity. As shown in Fig. 6b, Dam MTase activity gradually reduced under 5-fluorouracil treatment, and the half-maximal inhibitory concentration (IC_{50}) of 5-fluorouracil was calculated as 0.47 μmol/L, which was consistent with the previous reports [61,62,65]. These results demonstrated that the proposed system can be widely applied to screen targeted DNA MTase inhibitors.

In summary, we developed a dual signal-amplified ECL biosensor for the quantitative determination of Dam MTase by coupling TdT-mediated template-free branched polymerization for ECL emitter capture and WO_{3-x} dots-encapsulated MOFs (NH_2-UIO66@WO_{3-x}) as co-reactants. By applying NH_2-UIO66@WO_{3-x} as co-reactants for the ECL of Ru(phen)$_3$Cl$_2$, a 7-fold higher ECL intensity was observed compared to that using the individual WO_{3-x} dots as co-reactants. Moreover, the ECL biosensor showed a 20-fold enhanced ECL signal using TdT-mediated branched polymerization for the promoted capture of ECL emitters. The constructed ECL biosensor platform was not only suitable for both spiked serum samples and *E. coli* cells but also could screen potential inhibitors. This study provides a promising analytical platform for Dam MTase activity evaluation and inhibitor screening in the fields of clinical diagnosis and drug development.

Ethical statement

The human serum specimens were obtained from Zhongda Hospital (Nanjing, China) without any sample pretreatment except a dilution step, the human studies were reviewed and approved by the Independent Ethics Committee (IEC) for Clinical Research of the Affiliated Zhongda Hospital of Southeast University.

Delaration of competing interest

The authors declare no conflicts of interest.

Acknowledgment

This study was supported by the National Natural Science Foundation of China (Nos. 22074015 and 22174014).

Supplementary materials

Supplementary material associated with this article can be found, in the online version, at doi:10.1016/j.cclet.2023.108753.

References

[1] R.D. Scavetta, C.B. Thomas, M.A. Walsh, et al., Nucleic Acids Res. 28 (2000) 3950–3961.
[2] X. Cheng, R.J. Roberts, Nucleic Acids Res. 29 (2001) 3784–3795.
[3] Y. Yang, J.S. Yuan, J. Ross, et al., Arch. Biochem. Biophys. 448 (2006) 123–132.
[4] L.J. Smyth, E.H. Dahlstrom, A. Syreeni, et al., Nat. Commun. 13 (2022) 7891.
[5] E.M. Nickels, S. Li, S.S. Myint, et al., Nat. Commun. 13 (2022) 6077.
[6] S. He, L. He, B. Liu, et al., Chin. Chem. Lett. 30 (2019) 1031–1034.
[7] F. Rodriguez, I.A. Yushenova, D. DiCorpo, I.R. Arkhipova, Nat. Commun. 13 (2022) 1072.
[8] J. Casadesus, D. Low, Microbiol. Mol. Biol. Rev. 70 (2006) 830–856.
[9] D. Wion, J. Casadesus, Nat. Rev. Microbiol. 4 (2006) 183–192.
[10] K. Mutze, R. Langer, F. Schumacher, et al., Eur. J. Cancer 47 (2011) 1817–1825.
[11] V. Singh, P. Sharma, N. Capalash, Curr. Cancer Drug Targets 13 (2013) 379–399.
[12] Z.M. Li, X.L. Zhong, S.H. Wen, et al., Sens. Actuator. B: Chem. 281 (2019) 1073–1079.
[13] F. Li, Y. Chen, J. Shang, et al., Anal. Chem. 94 (2022) 4495–4503.
[14] P. Liu, M. Liu, H. Yin, et al., Sens. Actuator. B: Chem. 220 (2015) 101–106.
[15] H. Li, J. Wang, X. Wang, et al., ACS Appl. Mater. Interfaces 11 (2019) 16958–16964.
[16] W. Miao, Chem. Rev. 108 (2008) 2506–2553.
[17] Y. Zhao, L. Bouffier, G. Xu, et al., Chem. Sci. 13 (2022) 2528–2550.
[18] E.L. Yang, H. Yang, Z.Q. Ning, et al., Anal. Chem. 94 (2022) 16510–16518.
[19] Z. Wang, H. Gao, P. Liu, et al., Chin. Chem. Lett. 33 (2022) 3456–3460.
[20] Y. Li, S. Huang, S. Peng, et al., Small 19 (2022) 2206126.
[21] X. Huang, B. Li, Y. Lu, et al., Angew. Chem. Int. Ed. 62 (2022) e202215078.
[22] S. Yu, Y. Du, X. Niu, et al., Nat. Commun. 13 (2022) 7302.
[23] J. Ye, G. Liu, M. Yan, et al., Anal. Chem. 91 (2019) 13237–13243.
[24] Y. Liu, W. Guo, B. Su, Chin. Chem. Lett. 30 (2019) 1593–1599.
[25] Y. Song, X. Tao, W. Liang, et al., Chin. Chem. Lett. 34 (2023) 107957.
[26] X. Liu, L. Shi, W. Niu, et al., Angew. Chem. Int. Ed. 46 (2007) 421–424.

[27] N. Wang, H. Gao, Y. Li, et al., Angew. Chem. Int. Ed. 60 (2021) 197–201.
[28] D. Pan, Z. Fang, E. Yang, et al., Angew. Chem. Int. Ed. 59 (2020) 16747–16754.
[29] J. Zhao, Q. Shi, S. Luan, et al., J. Membr. Sci. 369 (2011) 5–12.
[30] J. Zhao, Y. He, K. Tan, et al., Anal. Chem. 93 (2021) 12400–12408.
[31] Y.M. Lei, J. Zhou, Y.Q. Chai, et al., Anal. Chem. 90 (2018) 12270–12277.
[32] C.J.T. Robidillo, J.G.C. Veinot, ACS Appl. Mater. Interfaces 12 (2020) 52251–52270.
[33] W.C. Chan, S. Nie, Science 281 (1998) 2016–2018.
[34] Y. Chen, G. Li, W. Mu, et al., Anal. Chem. 95 (2023) 3864–3872.
[35] G. Li, C. Wang, Y. Chen, et al., Small 19 (2023) 2206868.
[36] D. Zhu, Y. Zhang, S. Bao, et al., J. Am. Chem. Soc. 143 (2021) 3049–3053.
[37] S. Li, L. Wang, H. Su, et al., Adv. Funct. Mater. 32 (2022) 2200733.
[38] J. Xu, J. Ma, Y. Peng, et al., Chin. Chem. Lett. 34 (2023) 107527.
[39] Y. Shu, T. Su, Q. Lu, et al., Anal. Chem. 93 (2021) 16222–16230.
[40] R.P. Ojha, P.A. Lemieux, P.K. Dixon, et al., Nature 427 (2004) 521–523.
[41] Z. Wang, C.Y. Zhu, J.T. Mo, et al., Angew. Chem. Int. Ed. 58 (2019) 9854–9859.
[42] X.L. Tao, M.C. Pan, X. Yang, et al., Chin. Chem. Lett. 33 (2022) 4803–4807.
[43] X. Shi, H.M. Meng, X. Geng, et al., ACS Sens. 5 (2020) 3150–3157.
[44] C. Yang, K. Wang, Z. Li, et al., Sens. Actuator. B: Chem. 359 (2022) 1315593.
[45] L. Wen, L. Chen, S. Zheng, et al., Adv. Mater. 28 (2016) 5072–5079.
[46] Y. Wang, X. Wang, Y. Xu, et al., Small 13 (2017) 1603689.
[47] X. Shi, X. Lian, D. Yang, et al., Dalton Trans. 50 (2021) 17953–17959.
[48] Z. Wang, Y. Tian, W. Fang, et al., ACS Appl. Mater. Interfaces 13 (2021) 3166–3174.
[49] X. Wang, Y. Qi, Y. Shen, et al., Sens. Actuator. B: Chem. 310 (2020) 127756.
[50] X. Zhang, Y. Yang, P. Qin, et al., Chin. Chem. Lett. 33 (2022) 903–906.
[51] G. Gao, J.H. Chen, C.J. Li, et al., Anal. Chem. 94 (2022) 15856–15863.
[52] M. Zhao, Z. Huang, S. Wang, et al., ACS Appl. Mater. Interfaces 11 (2019) 46973–46983.
[53] J.H. Cavka, S. Jakobsen, U. Olsbye, et al., J. Am. Chem. Soc. 130 (2008) 13850–13851.
[54] V. Guillerm, S. Gross, C. Serre, et al., Chem. Commun. 46 (2010) 767–769.
[55] Q. Zhou, G. Li, K. Chen, et al., Anal. Chem. 92 (2020) 983–990.
[56] L. Yu, L. Zhu, Y. Peng, et al., Anal. Chem. 94 (2022) 11368–11374.
[57] Y. He, Y. Liu, L. Cheng, et al., ACS Appl. Mater. Interfaces 13 (2021) 298–305.
[58] H. Wang, F. Wang, T. Wu, Y. Liu, Anal. Chem. 93 (2021) 15794–15801.
[59] W. Miao, J.P. Choi, A.J. Bard, J. Am. Chem. Soc. 124 (2002) 14478–14485.
[60] H. Yang, Y. Zhang, Z. Yu, et al., Chin. Chem. Lett. 34 (2023) 107536.
[61] X. Xu, L. Wang, W. Cui, W. Jiang, Sens. Actuator. B: Chem. 266 (2018) 124–130.
[62] L.J. Wang, X. Han, C.C. Li, C.Y. Zhang, Chem. Sci. 9 (2018) 6053–6061.
[63] Y.C. Du, S.Y. Wang, X.Y. Li, et al., Biosens. Bioelectron. 145 (2019) 111700.
[64] X. Chen, G. Cao, X. Wang, et al., Biosens. Bioelectron. 163 (2020) 112271.
[65] Y. Han, C. Wang, X. Zou, et al., Anal. Chem. 94 (2022) 5980–5986.